Atoms **2015**, *3*, 433-449; doi:10.3390/atoms3030433

OPEN ACCESS
atoms
ISSN 2218-2004
www.mdpi.com/journal/atoms

Article

A Realization of a Quasi-Random Walk for Atoms in Time-Dependent Optical Potentials

Torsten Hinkel, Helmut Ritsch and Claudiu Genes *

Institut für Theoretische Physik, Universität Innsbruck, Technikerstrasse 25, Innsbruck A-6020, Austria; E-Mails: torsten.hinkel@student.uibk.ac.at (T.H.); helmut.ritsch@uibk.ac.at (H.R.)

* Author to whom correspondence should be addressed; E-Mail: claudiu.genes@uibk.ac.at.

Academic Editors: Jonathan Goldwin and Duncan O'Dell

Received: 30 June 2015 / Accepted: 15 September 2015 / Published: 23 September 2015

Abstract: We consider the time dependent dynamics of an atom in a two-color pumped cavity, longitudinally through a side mirror and transversally via direct driving of the atomic dipole. The beating of the two driving frequencies leads to a time dependent effective optical potential that forces the atom into a non-trivial motion, strongly resembling a discrete random walk behavior between lattice sites. We provide both numerical and analytical analysis of such a quasi-random walk behavior.

Keywords: cavity QED; optomechanics; random motion

1. Introduction

Over the past few decades, the optical control of motional degrees of freedom has seen great progress both on the experimental and theoretical fronts. As a particular example of such achievement, the cavity QED setting provides a paradigm for the observation and manipulation of motion of atoms, ions or atomic ensembles via tailored cavity modes [1–5]. In such a system, the time delay between the action of the field onto the atomic system's motion via the induced optical potential and the back-action of the particle's position change onto the cavity field leads to effects such as cooling [6–8] or self-oscillations (for a recent review see [9]). Addressing of the particle's motion works best for quantum emitters with sharp transitions such as ions or atoms but manipulation via the effective static polarizability is also possible in the case of molecules in standing wave [10] or ring cavities [11], or macroscopic particles such as levitated dielectric micron-sized spheres [12–14]. Typically, the driving is done either by direct pumping into the cavity mode via one of the side mirrors (longitudinal pumping), or indirectly via light

scattering off the atom into the field mode (transverse pumping). For transverse pumping, an exotic phenomenon dubbed as self-organization can occur in the many atom case [15]. Combinations of the two techniques (as depicted in Figure 1) have been theoretically investigated in the limit of equal laser frequencies [16]; in such a case, in a properly chosen rotating frame the effective combined optical potential can be rendered time independent and the analysis greatly simplifies.

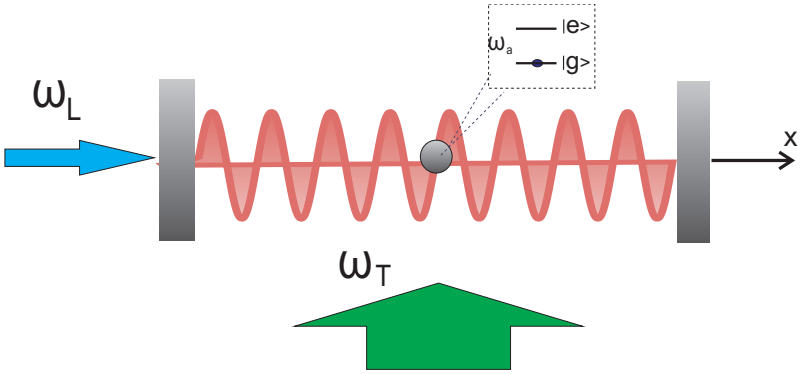

Figure 1. Schematics. Illustration of the model considered involving an atom moving inside an optical cavity with longitudinal driving of strength η_L and frequency ω_L and transverse driving η_T and frequency ω_T. The interference between the longitudinally pumped field and the field scattered from the transverse pump into the cavity mode leads to an effective optical potential that has a time dependent part oscillating at the frequency difference $\delta_T = \omega_L - \omega_T$.

Here we depart from this scenario to consider frequency beatings between the two pumps. While dynamics in the regime, where each pump acts alone, is well understood, extra forces arise from the interference between photons of different frequencies: (i) scattered from the transverse light field and (ii) entering the cavity mode from the longitudinal pump. The immediate effect of this interference force is to generate a time-dependent optical potential with a time modulation leading to a sign change that effectively induces the particle into undergoing jumps along the cavity sites in a quasi-random walk fashion. We analyze such a regime both numerically and via simplified analytical models. The mechanism is reminiscent of the one exploited in the creation of artificial potentials in optical lattices [17] applied here to the classical regime. By discretizing the trajectories, we analyze the emerging discrete process via its correlation function and find that it corresponds to an environment with a very short memory. The goal of this analysis is to provide a quantum optical setting in which the classical random walk can be observed and which would constitute a starting point into further generalizations into the quantum regime. In this sense, this work is a stepping stones towards a proposal for implementing a quantum random walk mirroring progress already achieved with photons [18], atoms in optical lattices [19], ions in traps [20] or on a one-dimensional lattice of superconducting qubits [21]. Our analysis is mainly based on a single two-level system but we discuss as well an extension involving doped micro-spheres where the field addresses a collective atomic variable (along the lines of hybrid optomechanics with doped mechanical resonators [22]).

The paper is organized as follows: in Section 2 we introduce the model. In Section 3 we present numerical evidence showing the occurrence of a quasi-random walk behavior and compute correlations of the engineered process that map close to those expected from a true random walk. In Section 4, we

present a simplified analytical model that allows us to derive the different forces acting on the particle and identify different regimes and associated scalings for the occurrence of the random walk. In Section 5, we discuss possible extensions of the model involving a tailored driving via a frequency comb laser. We conclude and present an outlook in Section 6.

2. Model

We consider the effective one-dimensional model depicted depicted in Figure 1 where an optical cavity mode at ω_c, decaying at rate κ is driven through a side mirror by a laser of amplitude η_L and frequency ω_L. Transversally, a second laser drives the atom directly with effective amplitude η_T at ω_T. The longitudinal mode spatial variation inside the cavity is $f(x) = \cos(kx)$ (k is the corresponding wave-vector for the light mode with wavelength $\lambda = 2\pi/k$) and the atom-photon coupling is specified by $g(x) = gf(x)$ (with g being the maximum coupling). The total system is described by the Hamiltonian

$$\hat{H} = \hat{H}_0 + \hat{H}_p + \hat{H}_{JC} \tag{1}$$

consisting of a free part $\hat{H}_0$, a pumping term $\hat{H}_p$ and the Jaynes-Cummings interaction $\hat{H}_{JC}$. The free evolution Hamiltonian describes the dynamics of a free particle of mass m and momentum operator $\hat{p}$ plus that of the cavity mode (annihilation operator $\hat{a}$) and the two-level atom

$$\hat{H}_0 = \frac{\hat{p}^2}{2m} + \hbar\omega_c \hat{a}^\dagger \hat{a} + \frac{\hbar\omega_a}{2}\hat{\sigma}^z \tag{2}$$

The atom dynamics is described with the help of the Pauli operators $\hat{\sigma}^\pm$ and $\hat{\sigma}^z$ satisfying $[\hat{\sigma}^+, \hat{\sigma}^-] = \hat{\sigma}^z$ and $[\hat{\sigma}^\pm, \hat{\sigma}^z] = \mp 2\hat{\sigma}^\pm$. The atom's interaction with the cavity field is included as a Jaynes-Cummings photon-excitation exchange process quantified by the position dependent coupling strength $gf(x)$:

$$\hat{H}_{JC} = i\hbar g f(x)(\hat{\sigma}^+ \hat{a} - \hat{a}^\dagger \hat{\sigma}^-) \tag{3}$$

Finally driving is included in the pump terms

$$\begin{aligned} \hat{H}_p =& i\hbar\eta_L(\hat{a}^\dagger e^{-i\omega_L t} - \hat{a}e^{i\omega_L t}) + \\ & i\hbar\eta_T(\hat{\sigma}^+ e^{-i\omega_T t} - \hat{\sigma}^- e^{i\omega_T t}) \end{aligned} \tag{4}$$

including direct pumping into mode $\hat{a}$ and atom driving of the dipole operator $\hat{\sigma}^-$.

We proceed in a standard way to derive equations of motion for classical quantities [23]. First, we make a set of transformations to dimensionless normalized position $x = k\langle\hat{x}\rangle$ and momentum $p = \langle\hat{p}\rangle(\hbar k)^{-1}$. We denote the field amplitude by $\alpha = \langle\hat{a}\rangle$ and the averaged atomic polarization by $\beta = \langle\sigma^-\rangle$ (in a frame rotating at ω_L). In a first stage we consider finite saturations of the population difference operator $\hat{\sigma}^z$ whose classical average we denote by β^z. We furthermore assume that the build-up of quantum correlations between the atom and the photon field can be neglected so that we can replace the nonlinear terms such as $\hat{a}\hat{\sigma}^z$ by their factorized classical averages $\alpha\beta^z$. The complete equations of motion for atom and field are (including the dissipative dynamics of the field mode at rate κ and of the atomic coherence at rate γ):

$$\dot{\alpha} = (-\kappa + i\Delta_c)\alpha - gf(x)\beta + \eta_L \tag{5}$$

$$\dot{\beta} = (-\gamma + i\Delta_a)\beta - gf(x)\alpha\beta^z - \eta_T\beta^z e^{i\delta_T t} \tag{6}$$

$$\dot{\beta}^z = -2\gamma(\beta^z + 1) - 4gf(x)\mathrm{Re}\{\beta^*\alpha\} - 4\eta_T\mathrm{Re}\{\beta^* e^{i\delta_T t}\} \tag{7}$$

We introduced the detunings $\Delta_a = \omega_L - \omega_a$, $\Delta_c = \omega_L - \omega_c$ and $\delta_T = \omega_L - \omega_T$ (illustrated in Figure 2 with corresponding sign conventions).

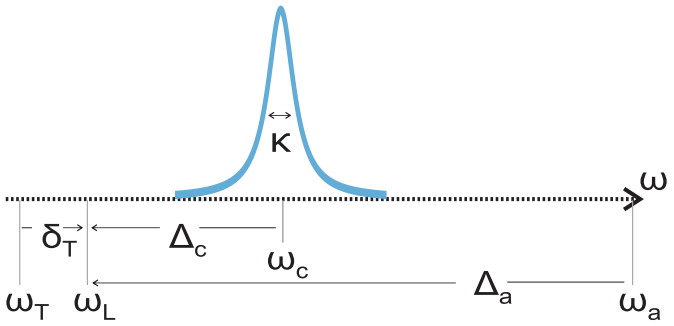

Figure 2. *Frequencies*. Illustration of the frequencies and detunings as defined/used in the equations of motion. The detunings are taken with respect to the longitudinal driving frequency such that $\Delta_c < 0$ corresponding to the stable regime of cavity QED with moving atoms (far from motional instability points) and $\Delta_a < 0$ that corresponds to $U_0 = g^2/\Delta_a < 0$ as for high-field seekers.

However, for the moment, we restrict our treatment to the low saturation case, where $|\beta|^2 \ll 1$ which allows us to linearize the $\hat{a}\sigma^z$ term by setting $\sigma^z \to -1$. Such a linearized regime allows one to analytically derive the forces acting on the particle. Numerical evidence points out that this simplified limit provides similar effects with the finite saturation case and we will base our analytical treatment on the following simplified system of equations:

$$\dot{\alpha} = (-\kappa + i\Delta_c)\alpha - gf(x)\beta + \eta_L \tag{8}$$

$$\dot{\beta} = (-\gamma + i\Delta_a)\beta + gf(x)\alpha + \eta_T e^{i\delta_T t} \tag{9}$$

The motion of the atom is described by

$$\dot{x} = 2\omega_r p \tag{10}$$

$$\dot{p} = -2gf'(x)\mathrm{Im}\{\alpha^*\beta\} \tag{11}$$

where we have condensed the particle's properties into the recoil frequency $\omega_r = \hbar k^2/(2m)$ and we have neglected spontaneous emission induced momentum diffusion.

3. The Quasi-Random Walk—Numerical Results

Before obtaining insight from analytical considerations, we start by simulating the dynamics of the system. This is achieved by fixing the set of parameters to: $\Delta_a = -1.5\kappa$, $\Delta_c = -1.5\kappa$, $\eta_L = \kappa$, $\delta_T = \frac{\pi}{100}\kappa$, $\gamma = \kappa$, $g = \kappa \times 10^{-2}$, $k = 2\pi$ and recoil frequency $\omega_r = 0.1\kappa$. We treat η_T as a free varying parameter. In the following we set $\kappa = 1$ for numerical simulations and normalize the time in units of κ^{-1}. We choose a regime described in the next analytical section as "trapping via longitudinal pump", where we first tune the parameters such that trapping of the particle is ensured in the absence of the transverse driving. We then increase η_T, and notice that past a given threshold, the particle starts jumping out of its trapping site to the neighboring left/right sites in an apparently random way.

In Figure 3 we exemplify such a trajectory obtained for a particle initialized with $p_0 = 0$ around the origin at $x_0 = 3.5 \times 10^{-3}$ and for $\eta_T = 0.55\kappa$.

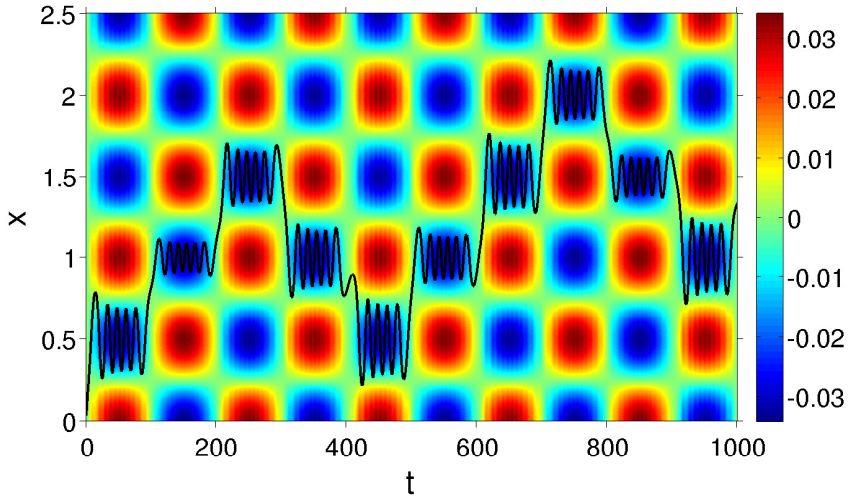

Figure 3. Quasi-random walk trajectory. A single trajectory (black curve) overlapped with the effective potential as a function of increasing time for lattice sites appearing at full and half integer values of x (with $\lambda = 1$). The optical potential is illustrated as colored background and oscillates in time with a period of $T = \pi/\delta_T$. Note that t is dimensionless as it is expressed in units of κ^{-1} and κ is set to unity.

3.1. Discrete Process—Single Trajectories

We then discretize the process by choosing time steps in units of the time period between two jumps T, which is half the period of the potential time oscillation. At $t_n = nT$ the particle is released from the potential and jumps to an adjacent trapping site. This is illustrated in Figure 4 as the transition from the continuous trajectories in the upper plot to the discrete plots of site number in the middle plot. The discrete positions (the locations of the sites) are defined as:

$$x_n \equiv \frac{1}{2T}\left[2\int_{t_{n-1}}^{t_n} dt x(t)\right] \tag{12}$$

where the square brackets stand for the rounding of the integral to the nearest integer, corresponding to the location of the site where trapping occurs.

With the parameters from above, we then analyze the dynamics as a function of randomized initial conditions; we initialize the particle with a momentum and position $(x_0, p_0) \in [-0.1, 0.1] \times [-0.1, 0.1]$ inside the potential well around zero and follow the evolution over time normalized to T for 10^3 initial values. First, we illustrate the mixing of trajectories, as shown in Figure 5, by color coding the trajectories starting with $x_0 > 0$ in green and those starting with $x_0 < 0$ in black. The mixing is evident and can be taken as a first indicator for randomness.

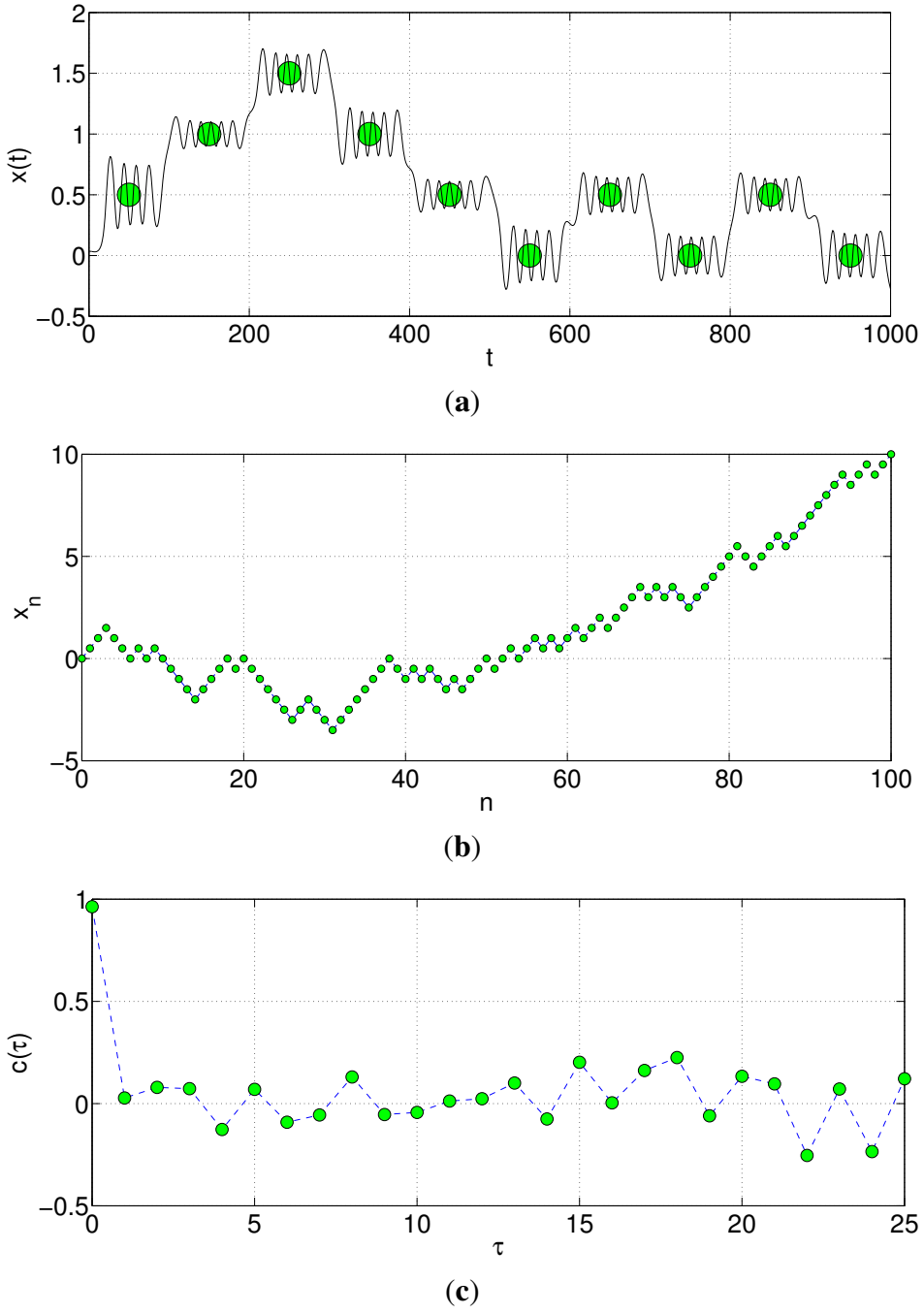

Figure 4. Discretization of the process. (**a**) Example of a single continuous trajectory plotted versus time and the corresponding discretized position as green dots in the center of one single well oscillation; (**b**) Corresponding discrete trajectory over 100 jumps, which conform to 10^4 time units, as a function of the jump index n; (**c**) Correlation function of the single trajectory from above as a function of time delay between two occurring jumps.

One can introduce the jump sequence $J_N = (j_1, j_2, ..., j_N)$, where the jump indicators are defined as $j_n = x_{n+1} - x_n$, and according to their sign show either left or right jump behavior. One can define the autocorrelation function for this process as

$$C_N(\tau) = \frac{1}{N-1} \sum_{n=1}^{N} (j_{n+\tau} - \langle j_n \rangle)(j_n - \langle j_n \rangle) \tag{13}$$

which characterizes the joint probability for the occurrence of jumps separated by a time delay τT. The behavior of this function for a single trajectory is shown in Figure 4c in the lower plot. By definition the zero time delay correlation is normalized to unity and it decreases to values around zero where negative values show anti-correlated jumps while positive values indicate correlated jumps.

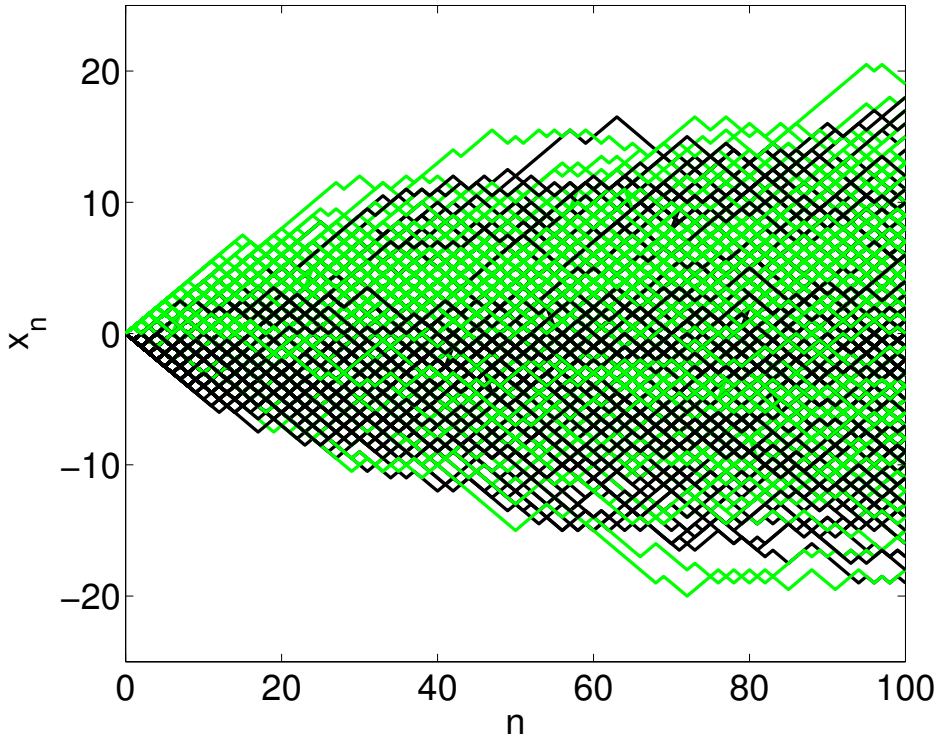

Figure 5. Mixing of trajectories. Simulation of 10^3 discrete trajectories $x_n(x_0)$ as a function of the jump number index n, starting with uniform distributed initial positions and momenta out of the interval $[-0.1, 0.1]$. The color coding refers to negative/positive initial positions (black/green): notice that the evolution completely mixes the negative and positive regions.

3.2. Discrete Process—Many Trajectories Statistics

We numerically simulate a large number of trajectories (with starting point around the origin) for 10^2 time steps and different values of the jump period T. The distribution of the final site occupancy is illustrated in Figure 6a–c. The histograms of all three cases coincide with binomial distributions expected from the classical random walk. The fitting is done with a Gaussian distribution, where the standard deviation of the histogram is considered as the distribution's width. The variance in position x of the unbiased binomial distribution is given by $\langle(\Delta x_n)^2\rangle = a^2 n$, where a is the constant spatial separation of adjacent lattice sites. Since the trapping positions in our model are separated by a distance of $\frac{\lambda}{2}$ and we set $\lambda = 1$, we expect a variance of $\langle(\Delta x_n)^2\rangle = \frac{1}{4}n$. The numerically observed variances in Figure 6d–f show a dependency of the slope of the linear increase, which is equivalent to the diffusion constant, on the jump period T.

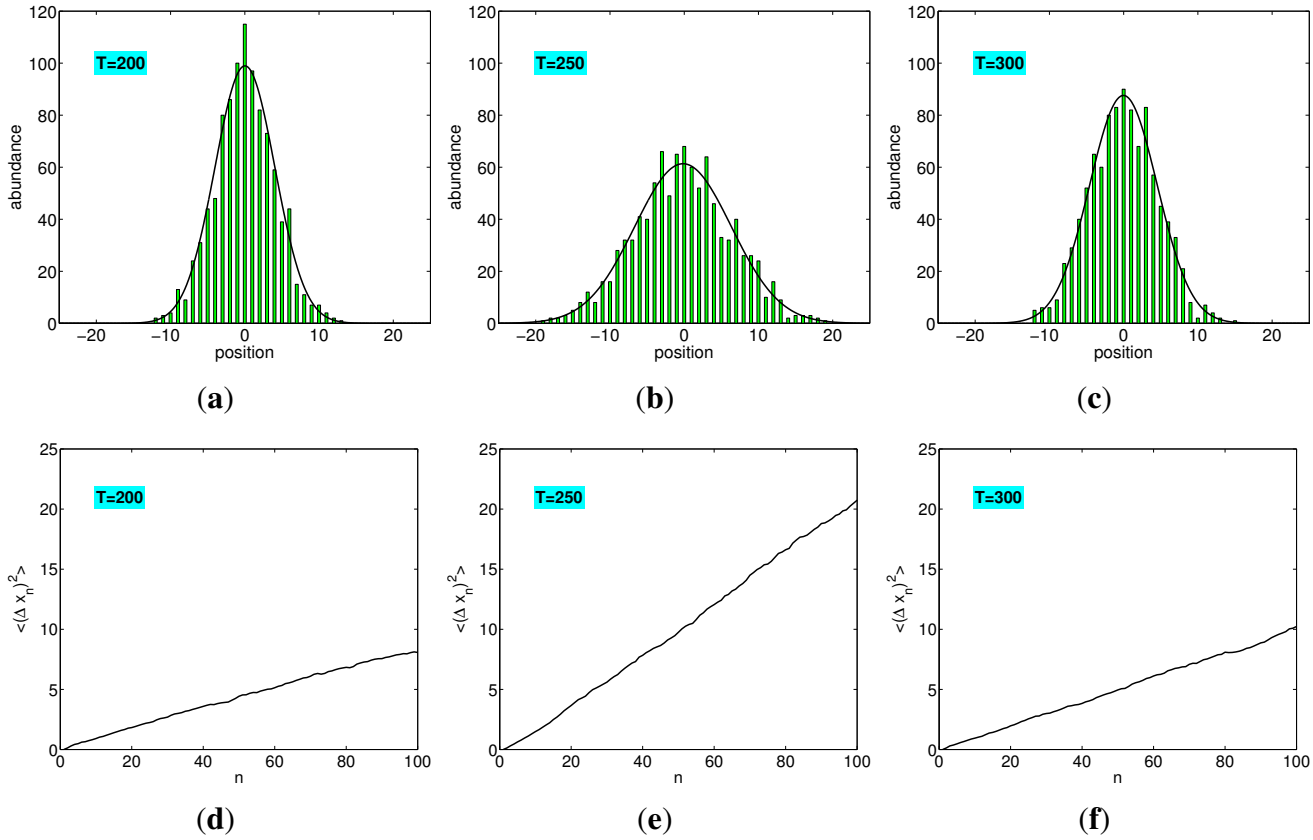

Figure 6. Final site occupancy and mean variances. (**a**)–(**c**) Histograms of populations of lattice sites at arrival. The arising distributions fit well with the expected binomial distribution (here the fit is with a Gaussian owing to the large number of steps considered $N = 100$) characteristic of a random walk. The standard deviations of the distributions vary with the time period T between two jumps. This corresponds to different diffusion constants, given by the slopes of the variance curves below; (**d**)–(**f**) Mean variance in position as a function of jump index n. The linear increase with the amount of steps reproduces the main property of a classical discrete one dimensional random walk. For $T = 250$ the slope is close to the expected value of 0.25 for a perfect random walk, while the other two cases show sub-diffusion.

The main result of the numerical section is however the behavior of the jump correlation function averaged over many trajectories (see Figure 7). For a perfect random walk process, the correlation function for jumps separated by $\tau > T$ would be vanishing. This corresponds to a reservoir having no memory. In our case for $T = 200$ and 300 however, short time delays (below 5 jumps) are anti-correlated while after around 5 jumps correlations occur. These anti-correlations do not occur in the second case, which shows the best coincidence with the expectation for a perfect random walk. The anti-correlations seem to correspond to sub-diffusion of the averaged particle motion as they favor jumps back to origin at given time distances which might inhibit the spread of the total motion.

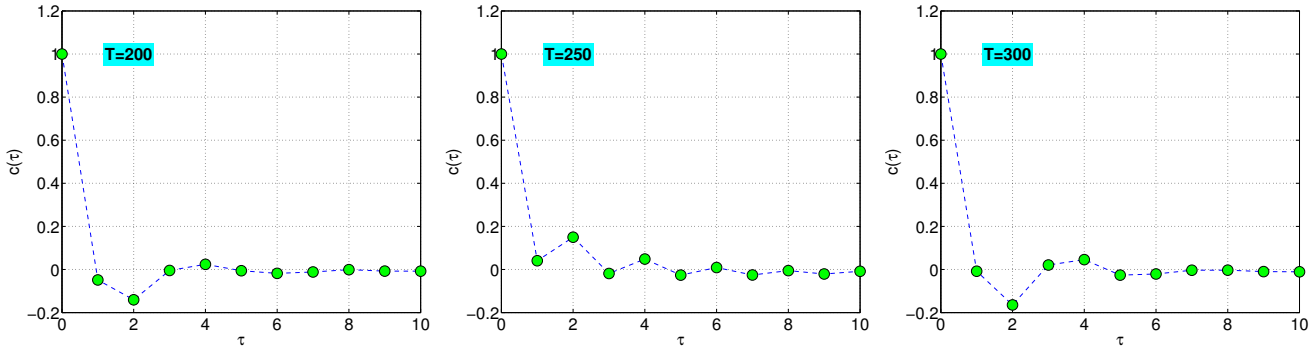

(**a**) (**b**) (**c**)

Figure 7. Averaged jump-correlations. Numerical data showing the variation of the correlation function with the delay time between jumps for different values of T. As a basis of comparison, the correlations of a pure random walk would correspond to a function reaching unity for $\tau = 0$ and zero elsewhere. On the given numerical example, the particle is subjected to an effective reservoir with a non-vanishing memory that allows for anti-correlations of jumps close to each other. These strong negative regions are missing in the middle case b) that corresponds to the highest diffusion.

To gain some physical understanding, one can inspect Equation (11) where the right-hand side represents the effective optical force. In some limit (revealed by the numerical results) this force shows effective quasi-random kicks whose correlations map onto the correlation function for the discrete process. For perfectly uncorrelated kicks the effect would be a random walk. However, in the realistic case some correlations between jumps remain. One can consider the following argument: the momentum kick at one site is the integral of the force over a time T during which the force varies non-trivially. In the continuous limit the process is deterministic. However, in the limit of many oscillations inside a single site, the phases of the momentum kicks occurring at different sites are randomized. On the other hand the numerical results show an alternating behavior of the system with T. The fact that e.g., the diffusion constant decreases again from $T = 250$ to $T = 300$ gives rise for the hypotheses that this system is more close to a random walk for special ratios of the phases of the single trapping site oscillations and the oscillation of the potential in time.

4. Analytical Results

The dynamics numerically derived in the previous section can be explained at least in some particular limits by a simplified model where the atomic and field degrees of freedom are eliminated and an effective set of equations is derived for the particle motion only. Let us first rewrite the effective force acting on the particle in the following form:

$$F(x,t) = -2f'(x)\mathrm{Im}\{\alpha^*(g\beta)\} \tag{14}$$

and proceed with finding analytical expressions in the adiabatic limit.

4.1. Elimination of the Atomic Dipole

Under the assumption of purely dispersive coupling brought by the weak, far off-resonance driving $\Delta_a \gg \gamma, \eta_T$ one can eliminate the atomic variable and compute

$$\begin{aligned} g\beta &\simeq i\frac{g^2}{\Delta_a}\alpha f(x) + i\frac{g\eta_\tau e^{i\delta_T t}}{\Delta_a} \\ &= iU_0\alpha f(x) + i\bar{\eta}_T e^{i\delta_T t} \end{aligned} \tag{15}$$

where the per photon dispersive coupling is given by $U_0 = g^2/\Delta_a$ and the effective transverse pump is defined as $\bar{\eta}_T = g\eta_T/\Delta_a$. Replacing the steady state value of β in the force expression we obtain:

$$F(x,t) = -2f'(x)f(x)U_0|\alpha|^2 - 2f'(x)\bar{\eta}_T \mathrm{Re}\{\alpha^* e^{i\delta_T t}\} \tag{16}$$

Notice that the first term is the well-known force arising from the longitudinal pump into the cavity. Combined with time-delay effects coming from the finite ring-down time of the cavity field, such a force can lead to cavity cooling, heating, bistability or self-oscillations [8,9]. The second term is of more importance in our treatment as it shows the interference between the two pumps and it contains the time-modulation needed for the potential sign change.

4.2. Elimination of the Field Variable

Since the time-delay effects do not play a role in the occurrence of jumps, we proceed by considering the limit of small U_0 where we eliminate the cavity field. Replacing β from Equation (15), leads to

$$\dot{\alpha} = \left[-\kappa + i(\Delta_c - U_0 f^2(x)\right]\alpha + \eta_L - i\bar{\eta}_T f(x) e^{i\delta_T t} \tag{17}$$

Under the assumption that $\eta_L, \bar{\eta}_T \ll \max(\kappa, \Delta_c)$ and defining a position dependent cavity detuning $\Delta_c - U_0 f^2(x) \equiv \Delta(x)$, one obtains:

$$\alpha = \frac{\eta_L - i\bar{\eta}_T f(x) e^{i\delta_T t}}{\kappa - i\Delta(x)} \tag{18}$$

We now can compute the cavity photon number

$$|\alpha|^2 = \frac{\eta_L^2 + \bar{\eta}_T^2 f(x)^2 + 2\eta_L \bar{\eta}_T f(x)\sin(\delta_T t)}{\kappa^2 + \Delta(x)^2} \tag{19}$$

as well as

$$\mathrm{Re}\{\alpha^* e^{i\delta_T t}\} = \frac{\eta_L\left[\kappa\cos\delta_T t + \Delta(x)\sin(\delta_T t)\right] + \Delta(x) f(x)\bar{\eta_T}}{\kappa^2 + \Delta^2(x)} \tag{20}$$

and replace these expressions in Equation (16).

4.3. Optical Forces

We can now group the different terms contributing to the total optical force acting on the particle as follows: (i) arising from the longitudinal field; (ii) from the transverse field and (iii) a time dependent interference term. Explicitly writing the three terms as $F(x,t) = F_L(x)+F_T(x)+F_{LT}(x,t)$, we compute

$$F_L = -2f'(x)f(x)\frac{\eta_L^2}{\kappa^2+\Delta^2(x)}U_0 \tag{21}$$

Which describes the standard $\cos^2(x)$ optical potential induced by the longitudinal pump. The next term is

$$F_T = -2f'(x)f(x)\frac{\bar{\eta}_T^2}{\kappa^2+\Delta^2(x)}\Delta_c \tag{22}$$

and it shows the effect of the time-independent interference between transverse pump photons and the particle scattered photons filling the cavity mode. The most interesting term is

$$\begin{aligned} F_{LT} =& 2f'(x)\frac{\bar{\eta}_T\eta_L}{\kappa^2+\Delta^2(x)}[\kappa\cos(\delta_T t) \\ &+ (\Delta_c + U_0 f^2(x))\sin(\delta_T t)] \end{aligned} \tag{23}$$

showing modulation in time at δ_T. Notice that the time independent limit can be reached by setting $\delta_T = 0$, and this force reduces to $2f'(x)\bar{\eta}_T\eta_L\kappa/(\kappa^2+\Delta^2(x))$.

4.4. Trapping by Interference

Let us consider the limit of small g and tune the driving field amplitudes such that $\eta_T \gg g\eta_L$ while at the same time $\eta_T \ll \eta_L\Delta_a/(g\Delta_c)$. To satisfy both conditions simultaneously one has to require $U_0\Delta_c \ll 1$. Under these conditions, the time interference force is dominant and gives rise to an effective time-modulated trapping potential. We neglect the spatial modulation $U_0 f^2(x)$ as well with respect to the larger Δ_c and obtain the total force on the particle simplified to:

$$F \simeq -2\sin(x)\frac{\bar{\eta}_T\eta_L\kappa}{\kappa^2+\Delta_c^2}\cos(\delta_T t - \phi_\Delta) \tag{24}$$

where the phase is defined as: $\phi_\Delta = \arctan\frac{\Delta_c}{\kappa}$. The equations of motion for the particle are those of a frequency modulated pendulum and similar to the ponderomotive force with an important difference in that the amplitude of the driving changes sign periodically. In the limit of good localization (where we can expand $\sin(x) \simeq x$) we identify this as a restoring force for an harmonic oscillator with a time dependent normal frequency. We can readily compute the maximum trapping frequency ω_{tr} as

$$\omega_{tr,LT}^2 = 4\omega_r\kappa\frac{\bar{\eta}_T\eta_L}{\kappa^2+\Delta_c^2} \tag{25}$$

The quasi-random walk behavior arises from the periodic force sign change which, after a number of oscillations at a given site (roughly proportional to $T/T_{tr,LT}$ where $T_{tr,LT} = 2\pi/\omega_{tr,LT}$) forces the particle to settle itself inside an adjacent well.

4.5. Trapping by Longitudinal Pumping

A different regime is reached when the F_L and F_{LT} contributions are of the same order of magnitude. We achieve this by first turning on the longitudinal pump and see that a trapping time-independent potential is established. Along the equilibrium points, the longitudinal trapping frequency is around:

$$\omega_{tr,L}^2 = 8\omega_r \frac{U_0 \eta_L^2}{\kappa^2 + \Delta_c^2} \tag{26}$$

Tuning up the transverse pump, a time modulation of the trap frequency is achieved and a threshold emerges for η_T (for a rough estimate one can equate the maxima of F_L and F_{LT}) after which the particle starts jumping to adjacent sites. Given the two different spatial modulations of the forces, $\sin(2x)$ *vs.* $\sin(x)$, a double well structured potential arises with frequencies:

$$\bar{\omega}_{tr,L}^2 = 8\omega_r \frac{\eta_L(U_0\eta_L \pm \eta_T)}{\kappa^2 + \Delta_c^2} \tag{27}$$

4.6. Brownian Motion for Non-Delta Correlated Forces

We have already observed that a low diffusion constant is connected to oscillations in the correlation function $C(\tau)$, namely negative parts showing anti-correlations of jumps. While in the previous sections we discussed the discrete random walk process, we move now to the continuum and test that for a process undergoing brownian motion, non-delta correlated forces can indeed give rise to sub-diffusive behavior (*i.e.*, the convergence of the variance in space as function of time to a linear function with a slope below the solution for a delta-correlated force). The ansatz that we take for the expressions of the force-correlations is suggested by the shape of the jump-correlation functions of the discrete process. We start by assuming a particle underlying the stochastic equation of motion

$$\frac{dv}{dt} = -\lambda v + \xi(t) \tag{28}$$

Following the derivation in [24] the variance in space is

$$\left\langle (\Delta x)^2 \right\rangle = \int_0^t dt' \int_0^t dt'' \phi(t')\phi(t'') \left\langle \xi(t')\xi(t'') \right\rangle \tag{29}$$

with $\phi(t') = \frac{1}{\lambda}(1 - e^{\lambda(t'-t)})$ and the analytical solution for $\langle \xi(t')\xi(t'') \rangle = 2d\delta(t' - t'')$ is

$$\left\langle (\Delta x)^2 \right\rangle = \frac{2d}{\lambda^2}(t - \frac{2}{\lambda}(1 - e^{-\lambda t}) + \frac{1}{2\lambda}(1 - e^{-2\lambda t})) \tag{30}$$

For large times (or large λ) the expression above converges to the expected linear dependence $\langle (\Delta x)^2 \rangle = \frac{2d}{\lambda^2} t$. In our units, this corresponds to the typical linear diffusion with a slope of $1/4$. We now compare this solution to the numerically calculated variance for a force-correlation function of Gaussian and exponential shape times a cosine modulation for different oscillation frequencies. The expressions that we test are

$$\langle \xi(t')\xi(t'') \rangle = 2d \left\{ \begin{array}{c} e^{-(t'-t'')^2/2\sigma^2} \\ e^{-|t'-t''|/\sigma} \end{array} \right\} \cos(\Omega(t' - t'')) \tag{31}$$

We keep the width for all test functions fixed on a value of $\sigma = 0.5$ and vary the oscillation frequency Ω from 0.5 to 2.0 in steps of size 0.5.

As seen in Figure 8, the anti-correlations for this continuous process drop the diffusion of the particle's motion drastically and thus lead to sub-diffusion as expected. One should consider the fact that in this scenario the correlation functions do not converge to delta functions in the limit of vanishing width and frequency since they are not normalized.

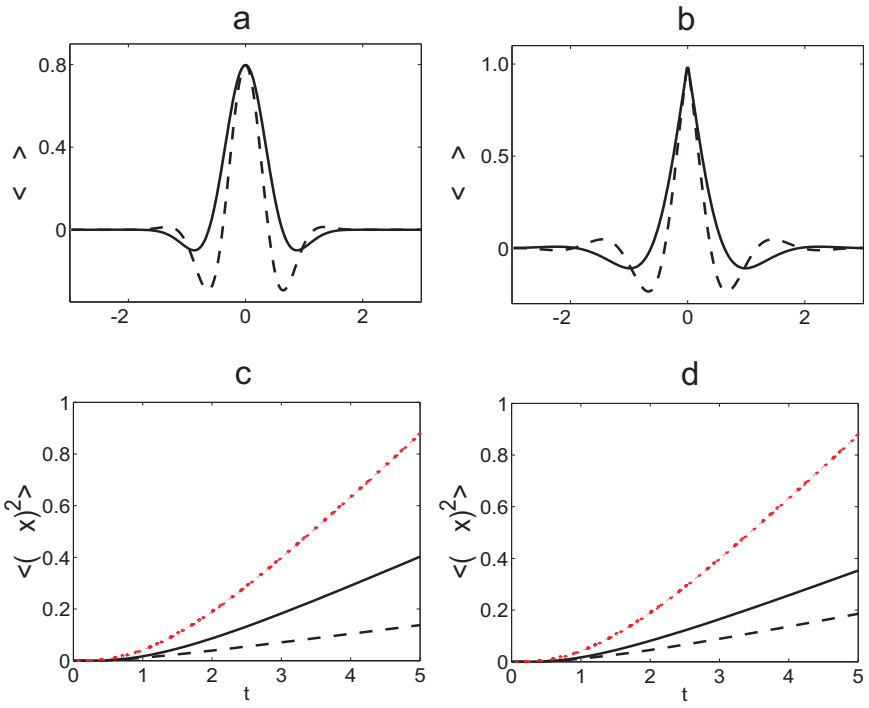

Figure 8. Force correlation functions and numerical solutions of the variance. (**a**),(**b**) Correlation as a function of time delay is illustrated for width $\sigma = 0.5$ and frequencies $\Omega = 0.5$ (black, full line) and 2.0 (black, dashed) for the Gaussian (left) and the exponential (right) case. The values of the local minima become lower as Ω increases and expand the segments of anti-correlation; (**c**),(**d**) Variances (same color pattern as above) converging to linear functions with slopes below the analytical solution (red dashed line).

5. Discussions

5.1. Frequency Comb Driving

In the limit where the pump interference provides the sole trapping mechanism, the force acting on the particle as in Equation (24) reminds of a parametrically driven pendulum. The dynamics consists of pendulum motion inside a given trap (which reduces to harmonic motion in the limit of good localization) with a time modulated frequency. However, one can engineer a multiple frequency transversal pumping scheme where the time modulation becomes a periodic kick instead of a sinusoidal function. To this end we consider a frequency comb driving (with $2N_f + 1$ frequencies) with the minimum frequency separation δ and centered at ω_L, such that the pump frequencies are $\omega_{T,j} = \omega_L - j\delta$. If we neglect

spontaneous atomic decay and the coupling between atom and cavity field, Equation (9) with the total pump term inserted gives

$$\dot{\beta}(t) \simeq i\Delta_a\beta + \eta_T \sum_{n=-N_f}^{N_f} e^{in\delta t} \tag{32}$$

In the limit $N_f \to \infty$ the driving on the right-hand side becomes a Dirac comb function. Inserting the steady state solution of Equation (32) together with $\alpha \simeq \eta_L$ into Equation (11) we get an equation of motion that maps onto the kicked rotor dynamics:

$$\dot{p} \simeq -\frac{\eta_L\bar{\eta}_T}{T_\delta}\sin(x)\sum_{n\in\mathbb{Z}}\delta(t-n\mathrm{T}) \tag{33}$$

where $T_\delta = 2\pi/\delta$. Together with Equation (11) the system can be exactly described via a transformation to the discrete and can be shown to exhibit chaotic motion past a threshold characterized by the tuning up of the force amplitude factor.

5.2. Hybrid Optomechanics with Doped Nano-Spheres

We can extend our treatment to consider a hybrid optomechanical system where we replace the two level system with a doped nano-sphere containing a collection of N such systems. We assume the nano-sphere transparent to light except for the doped part where the cavity mode excites a transition close to resonance. Let us consider the nano-particle of mass M with radius much smaller than specific length in which the cavity mode changes considerably (the cavity mode wavelength). The light-matter interaction takes place via the Tavis-Cummings Hamiltonian, that changes from the single atom picture in that $\hat{\sigma}^{\pm}$ is replaced by $\sum_j \hat{\sigma}_j^{\pm} \equiv S^{\pm}$. In the bosonic limit, where the saturation is very low, we can assume that $[S^-, S^+] = -N$ and proceed to write equations for averages ($\beta_N = \langle\hat{S}^-\rangle$):

$$\dot{\alpha} = (-\kappa + i\Delta_c)\alpha - gf(x)\beta_N + \eta_L \tag{34}$$

$$\dot{\beta_N} = (-\gamma + i\Delta_a)\beta_N + gNf(x)\alpha + N\eta_T e^{i\delta_T t} \tag{35}$$

The immediate gain in this approach from the single atom approach is the relaxation of the requirement of $|\beta|^2 \ll 1$ that turns into $|\beta_N|^2 \ll N$. However one has to pay the price of a reduced recoil frequency owing to an increased mass at least N times larger. The upshot is that a cavity QED regime, where we would expect a quasi-random walk with a macroscopic particle, can be unraveled.

5.3. Implementation Considerations

To experimentally observe the proposed quasi random walk, we advance a possible two step experimental procedure: (i) turn on longitudinal pumping detuned by $-\kappa$ from the resonance such that cavity cooling takes place in the absence of transverse pumping and (ii) turn on η_T past the threshold such that jumps are initiated. The typical cooling procedure can ideally cool the particle towards a thermal wavepacket with minimum energy $\hbar\kappa$ divided between the position and momentum quadratures (according to the thermal equipartition principle). In terms of normalized momentum and position initial variations this corresponds to $\delta p_0 = 1/\sqrt{2\omega_r}$ and $\delta x_0 = 1/(\sqrt{2U_0}\eta_L)$. For localization within a site

notice that we require $\delta x_0 \ll 1$ which results in $U_0 \eta_L^2 \gg 1$. This can be still fulfilled in the polarizable particle regime by tuning η such that $g^2/\Delta_a \ll 1$ while $g\eta_L \gg 1$.

6. Conclusions and Outlook

We considered the dynamics of particles (either as single two-level systems or sub-micron spheres doped with multiple emitters) inside time-dependent potentials resulting from interference in a two-color, two directional pump scheme. Past a given threshold, chaotic-like behavior can be observed, with correlations very close to those of a typical random walk. Depending on the beat frequency, the particles motion exhibits sub-diffusion that can be related to anti-correlations of the acting force. Analytically the system in the steady state can be reduced to a pendulum with a time dependent frequency modulation.

While the treatment here is in the classical regime, an immediate generalization into the quantum realm can be made by either: (i) treating motion classically and considering the effect of the quantum nature of the two-level system onto the dynamics or (ii) treating motion quantum mechanically and analyzing the dynamics of an initial wave packet, with direct connection to matter-wave interferometry applications. Another future direction aims to extend the 1D treatment to 3D dynamics where the beating of the two pumps give rise to an effective ponderomotive force. Investigations will be carried out on the possibility to exploit such a force for all optical trapping of polarizable particles (or realistic multilevel atoms) inside 3D optical cavities, similar to the mechanism employed in ion trapping inside linear Paul traps.

Acknowledgments

We thank Tobias Griesser for inspiring discussions. We acknowledge support from the Austrian Science Fund (FWF) via project P24968-N27 (C.G.) and via the SFB Foqus project F4013 and I1697-N27.

Author Contributions

Claudiu Genes has conceived the ideas and supervised the project. Torsten Hinkel conducted analytical calculations and performed numerical simulations. Helmut Ritsch provided guidance and expertise. All authors contributed to the writing of the manuscript.

Conflicts of Interest

The authors declare no conflict of interest.

References

1. Mabuchi, H.; Ye, J.; Kimble, H.J. Full observation of single-atom dynamics in cavity QED. *App. Phys. B* **1999**, *68*, 1095–1108.
2. Hood, C.J.; Lynn, T.W.; Doherty, A.C.; Parkins, A.S.; Kimble, H.J. The atom-cavity microscope: single atoms bound in orbit by single photons. *Science* **2000**, *287*, 1447–1453.

3. Maunz, P.; Puppe, T.; Schuster, I.; Syassen, N.; Pinske, P.W.H.; Rempe, G. Cavity cooling of a single atom. *Nature* **2004**, *428*, 50–52.
4. Leibrandt, D.R.; Labaziewicz, J.; Vuletić, V.; Chuang, I.L. Cavity Sideband Cooling of a Single Trapped Ion. *Phys. Rev. Lett.* **2009**, *103*, 103001.
5. Schleier-Smith, M.H.; Leroux, I.D.; Zhang, H.; van Camp, M.A.; Vuletić, V. Optomechanical Cavity Cooling of an Atomic Ensemble. *Phys. Rev. Lett.* **2011**, *107*, 143005.
6. Domokos, P.; Ritsch, H. Mechanical effects of light in optical resonators. *J. Opt. Soc. Am.* **2003**, *20*, 1098–1130.
7. Horak, P.; Hechenblaikner, G.; Gheri, K.M.; Stecher, H.; Ritsch, H. Cavity-Induced Atom Cooling in the Strong Coupling Regime. *Phys. Rev. Lett.* **1997**, *79*, 4974–4977.
8. Hechenblaikner, G.; Gangl, P.; Horak, P.; Ritsch, H. Cooling an atom in a weakly driven high-Q cavity. *Phys. Rev. A*, **1998**, *58*, 3030–3042.
9. Ritsch, H.; Domokos, P.; Brennecke, F.; Esslinger, T. Cold atoms in cavity-generated dynamical optical potentials. *Rev. Mod. Phys.* **2013**, *85*, 553–601.
10. Lev, B.L.; Vukics, A.; Hudson, E.R.; Sawyer, B.C.; Domokos, P.; Ritsch, H.; Ye, J. Prospects for the cavity-assisted laser cooling of molecules. *Phys. Rev. A* **2008**, *77*, 023402.
11. Schulze, R.; Genes, C.; Ritsch, H. Optomechanical approach to cooling of small polarizable particles in a strongly pumped ring cavity. *Phys. Rev. A* **2010**, *81*, 063820.
12. Romero-Isart, O.; Pflanzer, A.C.; Juan, M.L.; Quidant, R.; Kiesel, N.; Aspelmeyer, M.; Cirac, J.I. Optically levitating dielectrics in the quantum regime: Theory and protocols. *Phys. Rev. A* **2011** *83*, 013803.
13. Kiesel, N.; Blaser, F.; Delic, U.; Grass, D.; Kaltenbaek, R.; Aspelmeyer, M. Cavity cooling of an optically levitated submicron particle. *Proc. Natl. Acad. Sci. USA* **2013**, *11*, 14180–14185.
14. Asenbaum, P.; Kuhn, S.; Nimmrichter, S.; Sezer, U.; Arndt, M. Cavity cooling of free silicon nanoparticles in high vacuum. *Nat. Commun.* **2013**, *4*, 2743–2746.
15. Domokos, P.; Ritsch, H. Collective Cooling and Self-Organization of Atoms in a Cavity. *Phys. Rev. Lett.* **2002**, *89*, 253003.
16. Niedenzu, W.; Schütz, S.; Habibian, H.; Morigi, G.; Ritsch, H. Seeding patterns for self-organization of photons and atoms. *Phys. Rev. A* **2013**, *88*, 033830.
17. Struck, J.; Ölschläger, C.; Weinberg, M.; Hauke, P.; Simonet, J.; Eckardt, A.; Lewenstein, M. Sengstock, K.; Windpassinger, P. Tunable gauge potentials. *Phys. Rev. Lett.* **2012**, *108*, 225304.
18. Bouwmeester, D.; Marzoli, I.; Karman, G.P.; Schleich, W.; Woerdman, J.P. Optical Galton board. *Phys. Rev. A* **1999**, *61*, 013410.
19. Dür, W.; Raussendorf, R.; Kendon, V.M.; Briegel, H.J. Quantum walks in optical lattices. *Phys. Rev. A* **2002**, *66*, 052319.
20. Travaglione, B.C.; Milburn, G.J. Implementing the quantum random walk. *Phys. Rev. A* **2002**, *65*, 032310.
21. Ghosh, J. Simulating Anderson localization via a quantum walk on a one-dimensional lattice of superconducting qubits. *Phys. Rev. A* **2014**, *89*, 022309.
22. Dantan, A.; Nair, B.; Pupillo, G.; Genes, C. Hybrid cavity mechanics with doped systems. *Phys. Rev. A* **2014**, *90*, 033820.

23. Cohen-Tannoudji, C.; Diu, B.; Laloe, F. *Quantum Mechanics*; Wiley: Paris, France, 1977; Volume 1, pp. 312–314.
24. Lax, M.; Cai, W.; Xu, M. *Random Processes in Physics and Finance*; Oxford University Press: Oxford, UK, 2006.